Lasers in Manufacturing Conference 2021

# Manufacturing knowledge: model instead of experience, a big step towards reproducibility and first-time-right in the production of complex component geometries using PBF-LB/M

Hannes Korn[a,*], Stefan Holtzhausen[b], Felix Gebhardt[a] ,Claudia Ortmann[c], Ralph Stelzer[b], Welf-Guntram Drossel[a]

[a]*Fraunhofer Institute for Machine Tools and Forming Technology IWU, Nöthnitzer Str. 44, Dresden 01187, Germany*
[b]*Technical University of Dresden, Institute of Machine Elements and Machine Design, Dresden 01062, Germany*
[c]*Mathys Orthopädie GmbH, An den Trillers Büschen 2, Mörsdorf 07646, Germany*

**Abtract**

The cost structure and geometry freedom of laser powder bed fusion (PBF-LB/M) holds great potential for lightweight-capabilities, customization and on-demand manufacturing of metal parts. Obstacles currently exist in first time right manufacturing and reliable reproducibility under changing process conditions. Reasons are the many setting variables (laser parameters, process parameters, scan strategy) and disturbance variables (powder batch, operator, ambient conditions), which have a difficult to quantify influence on the quality characteristics of the component (warpage, surface roughness, porosity).
Compared to the so far widespread experience based parameterization of the process, statistical modeling has great potential for describing and understanding quantitatively the effects of the setting- and disturbance variables on the quality characteristics. The influence of scan strategy and laser parameters on the warpage and surfaces of PBF-LB/M-components is evaluated on cantilever-like bridge specimens according to an optimized experimental plan. The relation between setting variables and quality characteristics is quantified in a linear model approach and its predictive power is evaluated.
Keywords: scan strategy; parameter development; statistical modeling; warpage; complex geometry

* Corresponding author. Tel.: +49-351-4772-2119; fax: +49-351-4772-2303.
*E-mail address:* hannes.korn@iwu.fraunhofer.de.

## 1. Introduction

In the PBF-LB/M, there are many setting variables in the various steps of the process chain. Many of them can be set specifically and with good repeatability with a low ease of adjustment. However, many variables have a concurrent influence on the production result and these parameters must be individually adjusted to each other. To make matters worse, the influence of the process parameters on the quality characteristics is also strongly influenced by the geometry (parameters) of the component. This impedes the financially sensible manufacturing tasks, however, which are primarily small quantities (first time right).

In order to be able to assess whether first time right production is possible and which parameterization is suitable, several partial questions must be answered beforehand: For example, it is relevant to evaluate the quantity of influence of the geometry parameters compared to the process parameters on the various quality characteristics of the component. This is because in first time right manufacturing, the geometry changes from component to component. Furthermore, the question arises as to which process parameters have the greatest influence on the respective quality characteristics: is it sufficient to adjust a few influential process parameters to each other and to leave the remaining parameters at standard values?

Two important target parameters for additive components are warpage and surface roughness: Manufacturing defects caused by warpage are a common reason why additive manufacturing of a particular part fails. Poor surface properties require expensive and time consuming post processing steps.

This work investigates whether the use of statistics-based modeling methods (linear regression models) is a suitable tool to quantify the influence of different geometric and process parameters on the quality characteristics warpage and surface roughness. Additionally this knowledge is systematized in such a way that it can be used for predictions of optimized parameter combinations for new components.

## 2. State of the art and research

### *2.1. Quality characteristics for additively manufactured components*

Next to Electron Beam Melting (EBM), the Laser Powder Bed Fusion (PBF-LB/M) process is primarily used for the additive manufacturing of metals. Due to high industrial interest and the associated intensive research, this manufacturing technology has been significantly developed in recent years and is now capable of producing high strength components with complex geometries [Bartlett 2019]. However, due to the high energy input of the laser during the melting of the metal powder, anisotropic residual stresses are formed, which can result in distortion, reduced geometric dimensional accuracy and delamination [Masoomi 2017]. Whether a component can be manufactured and, if so, what geometric dimensional accuracy is achieved depends largely on the induced residual stresses. The associated distortion is a significant criterion for component quality and the general acceptance of additive manufacturing of metal components. The formation of residual stresses can be influenced by support structures, process parameters (e.g. laser power, scanning speed), exposure strategy, material properties and component geometry [Bartlett 2019], which have complex interdependencies. Residual stresses can be reduced mainly by optimizing support structures and adjusting exposure strategies (arrangement of individual scan vectors) [Masoomi 2017]. In addition to the use of build plate heating, shorter scan vectors, for example, also lead to a smaller temperature gradient and thus to less thermally induced residual stresses [Kruth 2012] [Parry 2016].

In the production of overhangs and bridge structures, the achievable surface finish also plays a major role. This depends mainly on the overhang angle (90°: orthogonal to the build direction, 0°: lying in the build direction) as well as the choice of process parameters. Recent studies show that a roughness of Ra=12 µm is currently achievable [Xiang 2019]. Whip investigated the dependence of surface roughness on laser

parameters [Whip 2019]. The dependency can be explained by an increase in the size of the melt pool at smaller overhang angles [Sih and Barlow 2004]. Due to the lower thermal conductivity of the powder than in the fused state, the melt pool decreases above a critical size [Gatto 2014], causing surface defects. At the same time, the resulting heat accumulation causes increased warpage [Wang 2013]. Therefore, a material-dependent critical angle between 35° and 45° is introduced in the literature [Pakkanen 2016, Cloots 2017, Gebhardt 2019].

### *2.2. Development of manufacturing parameters*

In addition to the actual component geometry, the manufacturing process depends on a large number of adjustable process parameters. [Rehme 2010] identifies around 150 influencing variables, with the actual process parameters having a primary influence on the manufacturability of overhangs. These can be divided into system and component parameters [Gebhardt 2019]. Above all, the component parameters are determined by the local exposure strategy and the associated control of the scan vectors. Thus, the local energy input can be decisively controlled. A distinction is made between line energy [Wang 2013], area energy [Jiang 2020] and volume energy [Cloots 2017, Chen 2017]. [Chen 2017] was able to prove the influence of volume energy on the melt pool dimension. Also, the increasing irregularities in the melt pool shape at smaller overhang angles could be shown [Xiang 2019]. In general, efforts are currently being made to minimize the energy density introduced in the overhangs [Lin 2019, Shi 2019, Cloots 2017]. This makes it difficult to merge adjacent orbits [Mertens 2014, Chen 2017, Calignano 2020]. An iterative, experiment based approach is currently proposed for determining suitable parameter combinations [Chen 2017]. Suitable parameter combinations are usually combined into machine and material specific parameter sets. These always represent a trade-off, a geometry-specific adaptation of the parameters usually does not take place.

For the production of overhangs, different exposure strategies have also been investigated [Shi 2019, DePond 2018] whereby for overhang angles smaller than 45°, standard hatch exposure provides the worst results. Better results were obtained using island-hatch strategies. Multiple exposures [Shi 2019, Jiang 2020] with lower energy input or using scan vectors parallel to the overhang [Cloots 2013, Cloots 2017, Chen 2017] also improve the results.

### *2.3. Modeling in PBF*

In particular, the combination of microscopic and macroscopic effects makes physics based modeling approaches for PBF-LB/M difficult: approaches that pursue sufficiently accurate process simulation are often too computationally intensive to scale up to the millions of individual scan vectors in an additively manufactured component.

Statistical design of experiments (DoE) and regression analysis, which is frequently used in this context, supports the description of complex interrelationships of individual parameters by providing a systematic approach to system and process analysis using statistical methods [Wember 1999, Kleppmann 2008]. In the field of laser beam melting, such an investigation of correlations between parameters and quality characteristics is currently hardly common. However, initial findings on interactions of the influencing variables have already been shown [Huxol 2019], although earlier work using DoE was unable to achieve optimization due to insufficient knowledge of the parameters [Huxol 2017]. In principle, it is therefore recommended to evaluate the parameter space first in a screening phase [Huxol 2019]. Other works were able to demonstrate improvements in the laser steel melting process using DoE and regression models [Calignano 2014, Charles 2019, Cloots 2017, Piscopo 2019, Sun 2013].

## 3. Experimental setup

In this work, specimens are manufactured by varying various parameters and then determining the quality characteristics of warpage and surface roughness. Subsequently, regression models are built to predict warpage and surface roughness. The varied parameters include geometry parameters of the specimens, parameters of the exposure strategy during slicing and hatching and the laser parameters during manufacturing. On the one hand, an attempt is made to select parameter combinations in such a way that the specimens can also be successfully manufactured, and on the other hand to cover as large a test area as possible in order to derive transferable statements. For this purpose, a central test plan is built up around a set of standard parameters already known for the material and the machine and is supplemented by corner points and repeat samples. The test plan is set up manually.

### *3.1. Specimens and measurements*

A bridge-like specimen geometry is used for the experiments (cf. Figure 1). This consists of a base and a bridge section and functions like a cantilever: The residual stresses introduced into the specimen during fabrication of the bridge section result in distortion of the bridge section after wire erosion. The width of all bridge specimens is 2 mm. The feet of all specimens are 10 mm high and in their cross-section, each foot is exposed by exactly three individual scan vectors during fabrication. The order of this exposure is constant across all layers and is the same for all specimens. All feet are exposed with the same laser parameters: Laser power $P$ = 100 W, scan speed $v$ = 625 mm/s, focus diameter $d\_f$ = 100 µm.

In the bridge area itself some parameters are varied:

- Geometry: bridge length $l$ (1 mm – 5 mm), bridge heigth $h\_1$ (0,5 mm – 2 mm)
- Production preparation: hatch distance $d$ (70 µm – 130 µm), scan strategy (vectors orthogonal to bridge *S_CHkonvQ*, vectors rotated by 45°, direction alternating 90° from layer to layer *S_Chkonv*)

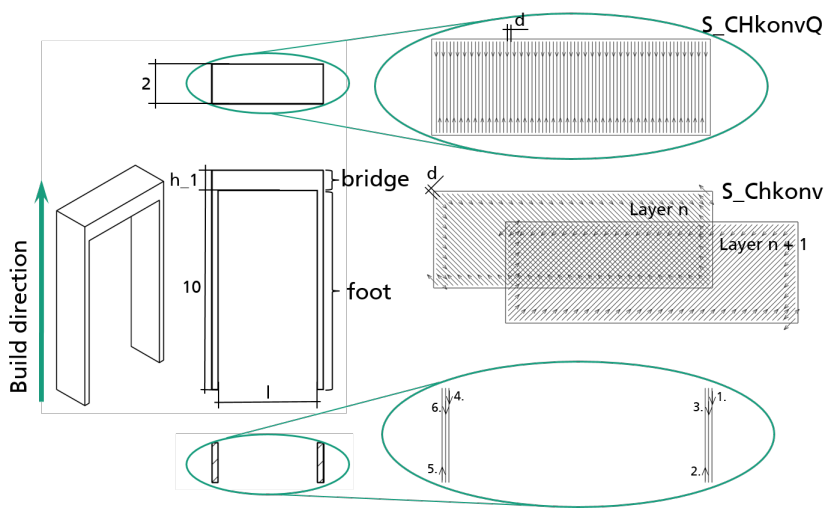


Fig. 1. Design, geometric parameters and parameters of the scan strategy of the used specimens.

Figure 2 shows which variables are measured on the specimens after fabrication and separation from the build plate by wire electronic discharge machining (wire EDM). The warping angle α (Fig. 2 (a)), line roughness and surface roughness (Fig. 2 (b)) are determined.

For the determination of the warping angle α, z-stack images (depth of field) of the laterally lying samples are taken using a digital microscope (Zeiss Smart Zoom 5, 34x zoom). The angles α are not measured directly. Instead, distances a, b, and c are measured in the microscope images. The warping angle α is calculated from these quantities according to formula (1).

$$\alpha = 2 \cdot \tan^{-1} \frac{b-a}{2 \cdot c} \tag{1}$$

The surface roughness is determined on a selection of 47 specimens from build job B (see section "3.2 Manufacturing") using a Keyence VR 5200 Profilometer (fringe projection). In each case, a line measurement of the roughness (measuring line 4 mm long) and an area measurement (1 mm x 2 mm) are carried out (cf. Figure 2 (b)) and *Rz*, *Ra*, *sz*, *sa* are determined from these within the Keyence software.

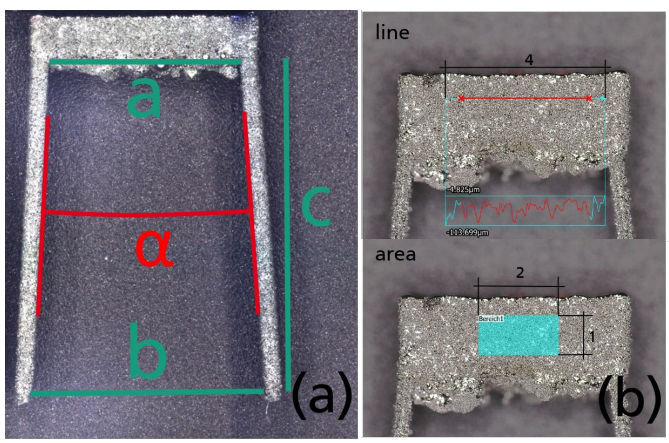


Fig. 2. (a) measured lines to calculate the warpage angle α; (b) line and area for measurement of the surface roughness

### *3.2. Manufacturing*

The specimens are manufactured on a Concept Laser M2 PBF/LB-M system from 2009 with retrofitted Focus Shift optics (minimum focus diameter: 55 µm). All specimens are produced in two build jobs (build job A, build job B) with identical arrangement on the build plate and directly one after another (same sieve batch of the powder). In a further build job (build job C), a selection of seven bridge specimens is produced with a time of more than six months inbetween to build job A and B using a different sieve batch to evaluate the predictive power of the model formed. The arrangement of the components on the build plate in build jobs A and B is shown in Figure 3 (a), the layer thickness is 25 µm in all build jobs. The material used is Ti6Al4V powder (manufacturer: TLS, order no. 1100710045). The particle size distribution of the batch sieved directly before production and characteristic values for the particle shape are shown in Figure 3 (b).

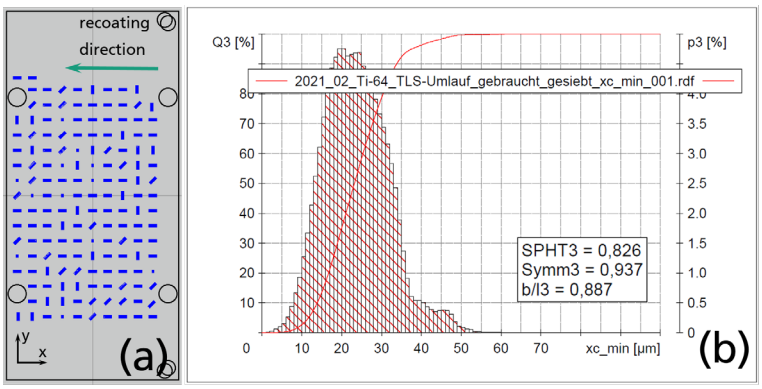


Fig. 3. (a) Specimens on the build job; (b) characteristics of the used powder

Following manufacturing parameters are deliberately varied:

- Component alignment: Rotation of the component around the z-axis (0° (longitudinal to recoater) - 90°)
- Laser parameters: Line energy *E* (0.1 J/mm - 0.22 J/mm), scan speed *v* (700 mm/s - 1500 mm/s), focus diameter *d_f* (55 µm - 150 µm)

In the experimental plan, the line energy *E* is varied specifically. However, the scanning speed *v* and laser power *P* are set on the PBF-LB/M machine. The laser power *P* is calculated from the line energy *E* and the scanning speed *v* according to formula 2 and thus lies between 70 W and 330 W:

$$P=E\cdot v \tag{2}$$

The specimens are positioned on the build plate in a grid and are randomly assigned to the individual positions in the grid. After production, the specimens are detached from the build plate by wire EDM at a height of 0.5 mm above the build plate.

### *3.3. Modeling*

The modeling is done using the software Cornerstone (camline GmbH, version 7.1). The modeling approach is linear regression with maximum quadratic terms. The approach makes model and scatter predictions with a 95% confidence interval.

This model approach was chosen because it can quantify possible correlations with relatively few individual measurements / samples. Furthermore, it is possible to make a direct statement about the expected scatter range for predictions based on this model. The approach also provides the possibility to check whether factors that are recorded but not considered in the model (e.g. component position on the build plate) have a systematic influence on the investigated target variables.

Overall, the performance of linear regression models in predicting the warping angle $\alpha$ (representative of warpage) is investigated by building four different models based on different data sets. A fifth model is built for the prediction of surface roughness. Table 1 lists the models considered and their main characteristics.

Table 1. Overview of the models taken into account.

| model name | order | database | prediction of |
|---|---|---|---|
| Model 1 | quadratic | build job A | warping angle |
| Model 2 | quadratic | build job B | warping angle |
| Model 3 | linear w/ interactions | build job A | warping angle |
| Model 4 | linear w/ interactions | build job B | warping angle |
| Model 5 | quadratic | build job B | roughness |

The same procedure is always used for the formation of the individual models 1 - 4: First, all actively varied input variables are included in the model formation. Then, the model is optimized by using Cornerstone's automatic model optimization tool with regard to the parameters "*Adj R-Square*" (What proportion of the occurring scatter can be explained by the model?) and "*RMS Error*" (Error to be expected in a forecast).

This procedure is also used for model 5 (roughness parameters), but in addition a Box-Cox plot is derived and the most favorable transformations are applied to the model functions for the target parameters *Rz*, *Ra*, *sz* and *sa*.

Models 1 - 4 are examined to determine whether the same parameters are included and whether they are attributed to a comparably large influence on the target variable of warping angle α (and thus residual stresses / distortion) by the respective model. From this, it is evaluated whether the mean of the linear regression models is also reliably suitable for identifying the parameters with the greatest influence on a target variable.

Furthermore, it is tested how well the models are suited for quantitative predictions of target variables. In each of the models 1 - 4, the parameter combinations that were used for the production of the respective components from build job C are used. Through the respective model, the expected warping angle *α* with its expected scatter limits is predicted. Subsequently, *α* measured after fabrication of the specimens is compared to these predictions.

Model 5 is used to try to find the explanatory parameters for the surface roughnesses that occur. The roughness parameters *Rz*, *Ra*, *sz* and *sa* are taken into account.

## 4. Results

In general, the build jobs A and B show almost identical distributions of the measured warping angles *α*. This indicates a very good reproducibility under identical process conditions. In the following, first the prediction of the warping angle by the different models and then the modeling for surface roughness will be discussed.

### *4.1. Warping angle*

All four models show a very high „*Adj R-Square*“ of more than 85% and indicate the average error to be about 1° (cf. Table 2). Thus, all four models hardly differ in this case with respect to their parameters „*Adj R-Square*“ and „*Pure Error*“. If we compare the two quadratic models, Model 1 and Model 2, we find that in both models hatch distance and scan strategy are identified as parameters with the greatest influence on the warping angle. In the linear models Model 3 and Model 4, scan strategy, hatch distance and bridge length l appear as the three most influential parameters.

Table 2. Key features of the resulting models.

| model name | Adj R-Square | Pure Error | Degrees of freedom | Three most significant Parameters (most influencial first) |
|---|---|---|---|---|
| Model 1 | 0,894 | 0,989 | > 125 | hatch distance, scan strategy, bridge length l |
| Model 2 | 0,877 | 1,098 | > 130 | hatch distance, scan strategy, bridge heigth h_1 |
| Model 3 | 0,888 | 0,989 | > 125 | scan strategy, hatch distance, bridge length l |
| Model 4 | 0,873 | 1,098 | > 135 | scan strategy, bridge length l, hatch distance |

The prediction of the expected warping angle $\alpha$ for specimens from build job C succeeds predominantly well. Figure 4 shows the predictions as well as the expected error intervals of the four models for $\alpha$ of seven specimens manufactured in build job C and compares them with the real angles measured on these specimens. Qualitatively, all models reproduce the real measured $\alpha$ very well. Quantitatively, it can be seen that the measured angles often lie outside the specified error intervals of the individual models.

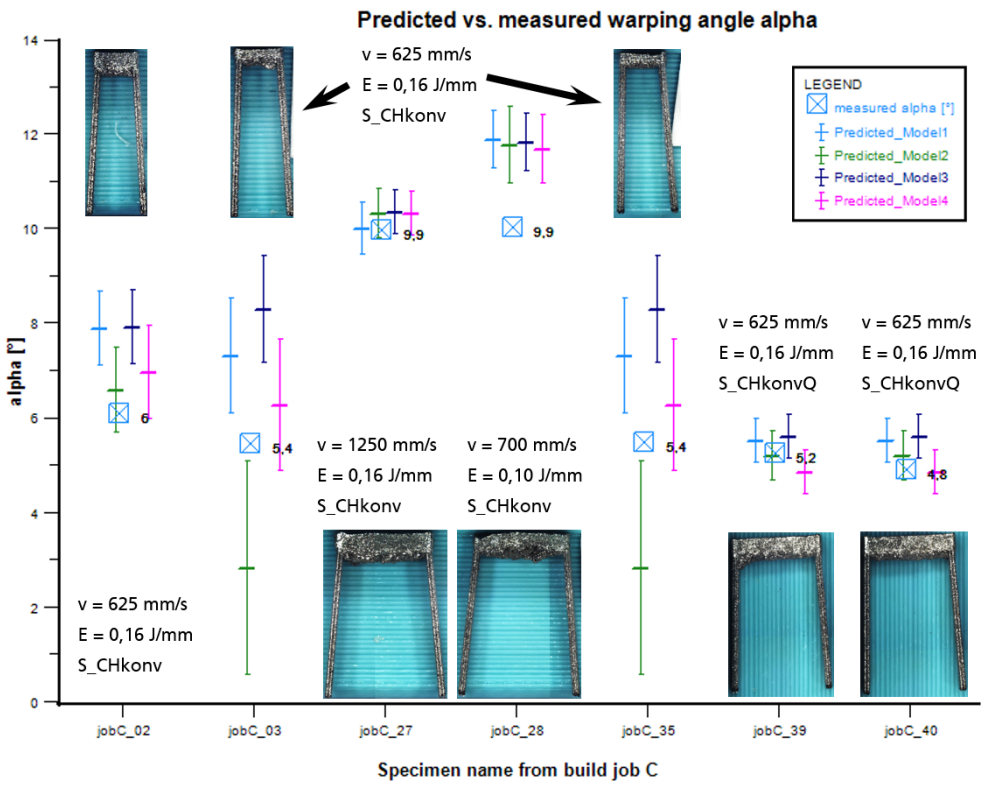


Fig. 4. Comparison between the predictions of the models 1 to 4 for the warping angle alpha and the measured warping angle of specimens built in build job C.

### *4.2. Surface characterization*

In contrast to the prediction of *α*, only models with very low *„Adj R-Square“* result for the modeling of the relationships between manufacturing parameters and surface roughness for the variables *Rz*, *Ra*, *sz* and *sa*. Thus, none of the models is suitable for a prediction of these surface parameters. Also a transformation of the models hardly improves this value. Table 3 shows the parameters for model 5 for the prediction of the transformed *Rz*, *Ra*, *sz* and *sa*.

Table 3. Adj R-Square for the surface parameters *Rz*, *Ra*, *sz*, and *sa* in model 5. Thus, none of the models is significant.

| predicted | Adj R-Square | degree of freedom |
|---|---|---|
| 1 / Rz | 0,212 | > 30 |
| Log Ra | 0,126 | > 30 |
| 1 / sa | 0,247 | > 30 |
| 1 / sz | 0,495 | > 30 |

## 5. Discussion

The experiments carried out show that even horizontal bridge elements can be manufactured if the process parameters are set specifically and the overhang area is supported on both sides.

In particular, it is striking that the warping angle hardly depends on the laser parameters, but primarily on the alignment of the scan vectors and the hatch distance. This is in accordance with the literature (e.g. [Parry 2016]). Just by adjusting the alignment of the scan vectors, a bridge with more than twice as long overhang area (jobC_39, jobC_40) can be manufactured with the same warpage as significantly shorter bridges with conventional arrangement of the hatches (jobC_02, jobC_03).

Furthermore, linear regression models seem to be very suitable to predict trends in the correlations between parameters and quality characteristics in PBF-LB/M and to find out which parameters have the greatest influence on various target variables. However, the confidence intervals estimated by the models in particular should be judged with caution. Especially at the edge of the considered parameter space, the predictive ability of the models may become significantly worse. Also, the use of regression models to investigate relationships between parameters and quality characteristics does not seem to be equally suitable for all quality characteristics. While for the warping angle α very good models could be found, the approach was not successful for surface roughness.

Several reasons can be considered for this: In modeling for surface roughness, there could be another source of scatter that was not taken into account in the model because it is not caused by the varied input variables. Similarly, it is conceivable that the surface parameters *Rz*, *Ra*, *sz*, and *sa* already scatter so much at the specified lengths that possible effects are to small to be identified. Likewise, it is possible that the parameters most influential for the surface roughness were not varied in a sufficiently large interval that their changes have a sufficiently large influence on the measured surface characteristics.

## 6. Outlook

In In the present work, the manufacturing results from two build jobs (A and B) were each used separately in the modeling, and samples from a third build job (C) were used to validate the predictions. In the future, it would be interesting to determine the prediction capabilities of the model by cross-validation instead of using a separate build job. This could either minimize the sample size and associated evaluation needed or create a more accurate model while maintaining the same predictive power.

Furthermore, it is planned to manufacture further bridge specimens under comparable conditions, but not to separate them from the build plate. Instead, the residual stresses on the undeformed specimens are to be measured by X-ray diffraction and correlated with the measured warping angles of comparable specimens. This would make it possible to quantify the residual stresses in SI units, even though only the easy-to-measure warping angle needs to be measured for future predictions.

An important follow-up step is also the investigation of the transferability of the results to other materials and PBF-LB/M systems. Further test series are necessary for this purpose. Likewise, the suitability of the means of modeling should also be investigated for other target variables, such as porosities in the material.

## Acknowledgements

This research and development project is funded by the German Federal Ministry of Education and Research (BMBF) within the Framework Concept “Zwanzig20 – partnership for innovation” in the consortium AGENT-3D (fund number 03ZZ0234B).

The authors also thank Merle Bergmann and Louise Elstner for making this work possible by providing microscope images and manually measuring hundreds of warping angles as well as doing the many surface characterizations that are the data basis for these investigations.

## References

Bartlett JL, Li X, 2019. An overview of residual stresses in metal powder bed fusion, Additive Manufacturing (2019), https://doi.org/10.1016/j.addma.2019.02.020

Calignano, Flaviana; Iuliano, Luca; Galati, Manuela; Minetola, Paolo; Marchiandi, Giovanni, 2020. Accuracy of down-facing surfaces in complex internal channels produced by laser powder bed fusion (L-PBF). Procedia CIRP 88, p. 423–426.

Calignano, F., 2014. Design optimization of supports for overhanging structures in aluminum and titanium alloys by selective laser melting. Materials & Design 64, p. 203–213.

Charles, Amal; Elkaseer, Ahmed; Thijs, Lore; Hagenmeyer, Veit; Scholz, Steffen, 2019. Effect of Process Parameters on the Generated Surface Roughness of Down-Facing Surfaces in Selective Laser Melting. Applied Sciences 9 (6), p. 1256.

Chen, Hongyu; Gu, Dongdong; Xiong, Jiapeng; Xia, Mujian, 2017. Improving additive manufacturing processability of hard-to-process overhanging structure by selective laser melting. Journal of Materials Processing Technology 250, p. 99–108.

Cloots, Michael; Zumofen, Livia; Spierings, Adriaan Bernardus; Kirchheim, Andreas; Wegener, Konrad, 2017. Approaches to minimize overhang angles of SLM parts. Rapid Prototyping Journal 23 (2), p. 362–369.

Cloots, M.; Spierings, A. B.; Wegener, K., 2013. Assessing new support minimizing strategies for the additive manufacturing technology SLM. Solid freeform fabrication proceedings. Austin, Texas, USA: University of Texas at Austin.

DePond, Philip J.; Guss, Gabe; Ly, Sonny; Calta, Nicholas P.; Deane, Dave; Khairallah, Saad; Matthews, Manyalibo J., 2018. In situ measurements of layer roughness during laser powder bed fusion additive manufacturing using low coherence scanning interferometry. Materials & Design 154, p. 347–359.

Di Wang; Yang, Yongqiang; Yi, Ziheng; Su, Xubin, 2013. Research on the fabricating quality optimization of the overhanging surface in SLM process. The International Journal of Advanced Manufacturing Technology 65 (9-12), p. 1471–1484.

Gatto, A.; Bassoli, E.; Denti, L.; Atzeni, E.; Iuliano, L.; Marchiandi, G. et al., 2014. Electro-discharge drilling on DMLS parts in Co-Cr-Mo alloy, p. 237–242.

Gebhardt, Andreas; Kessler, Julia; Schwarz, Alexander, 2019. Produktgestaltung für die Additive Fertigung. Hanser Verlag.

Huxol, Andrea; Villmer, Franz-Josef, 2019. DoE Methods for Parameter Evaluation in Selective Laser Melting. IFAC-PapersOnLine 52 (10), p. 270–275.

Huxol, A.; Scheideler, E.; Villmer, F.-J., 2017. Influencing Factors on Part Quality in Selective Laser Melting. Department of Production Engineering and Management, eds. Production Engineering and Management. Lemgo; 2017:13-34.

Jiang, Junjie; Chen, Jianming; Ren, Zhihao; Mao, Zhongfa; Ma, Xiangyu; Zhang, David Z., 2020. The Influence of Process Parameters and Scanning Strategy on Lower Surface Quality of TA15 Parts Fabricated by Selective Laser Melting. Metals 10 (9), p. 1228.

Kleppmann, Wilhelm, 2008. Taschenbuch Versuchsplanung: Produkte und Prozesse optimieren. 5., überarb. Aufl. München: Hanser (Praxisreihe Qualitätswissen).

Kruth, J.-P.; Deckers, J.; Yasa, E.; Wauthlé, R.; Wauthle, R., 2012. Assessing and comparing influencing factors of residual stresses in selective laser melting using a novel analysis method, Proc. Inst. Mech. Eng. Part B J. Eng. Manuf. 226 (2012) 980–991. http://dx.doi.org/10.1177/0954405412437085.

Lin, Kaijie; Yuan, Luhao; Gu, Dongdong, 2019. Influence of laser parameters and complex structural features on the bio-inspired complex thin-wall structures fabricated by selective laser melting. Journal of Materials Processing Technology 267, p. 34–43.

Masoomi, Mohammad; Thompson, Scott M.; Shamsaei, Nima, 2017. Laser powder bed fusion of Ti-6Al-4V parts. Thermal modeling and mechanical implications. In: International Journal of Machine Tools and Manufacture 118-119, p. 73–90. DOI: 10.1016/j.ijmachtools.2017.04.007.

Mertens, Raya; Clijsters, Stijn; Kempen, Karolien; Kruth, Jean-Pierre, 2014. Optimization of Scan Strategies in Selective Laser Melting of Aluminum Parts With Downfacing Areas. Journal of Manufacturing Science and Engineering 136 (6), p. 610-612.

Pakkanen, Jukka; Calignano, Flaviana; Trevisan, Francesco; Lorusso, Massimo; Ambrosio, Elisa Paola; Manfredi, Diego; Fino, Paolo, 2016. Study of Internal Channel Surface Roughnesses Manufactured by Selective Laser Melting in Aluminum and Titanium Alloys. Metallurgical and Materials Transactions A 47 (8), p. 3837–3844.

Parry, L.; Ashcroft, I.A.; Wildman, R.D., 2016. Understanding the effect of laser scan strategy on residual stress in selective laser melting through thermo-mechanical simulation, Addit. Manuf. 12 (2016) 1–15. http://dx.doi.org/10.1016/j.addma.2016.05.014.

Piscopo, Gabriele; Salmi, Alessandro; Atzeni, Eleonora, 2019. On the quality of unsupported overhangs produced by laser powder bed fusion. International Journal of Manufacturing Research 14 (2), p. 198.

Rehme, Olaf; Emmelmann, Claus; Morlock, Michael, 2010. Cellular design for laser freeform fabrication. 1. Aufl. Göttingen: Cuvillier (Schriftenreihe Lasertechnik).

Shi, Wentian; Wang, Peng; Liu, Yude; Han, Guoliang, 2019. Experiment of Process Strategy of Selective Laser Melting Forming Metal Nonhorizontal Overhanging Structure. Metals 9 (4), p. 385.

Sih, Samuel Sumin; Barlow, Joel W., 2004. The Prediction of the Emissivity and Thermal Conductivity of Powder Beds. Particulate Science and Technology 22 (4), p. 427–440.

Sun, Jianfeng; Yang, Yongqiang; Di Wang, 2013. Parametric optimization of selective laser melting for forming Ti6Al4V samples by Taguchi method. Optics & Laser Technology 49, pp. 118-124. DOI: 10.1016/j.optlastec.2012.12.002.

Wember, Theo, 1999. Technische Statistik und statistische Versuchsplanung - Einführung in statistische Methoden mit Anwendungsschwerpunkt in der Analyse technischer Daten. P & P Informationstechnologie GmbH, 1999

Whip, B., Sheridan, L. & Gockel, J, 2019. The effect of primary processing parameters on surface roughness in laser powder bed additive manufacturing. Int J Adv Manuf Technol 103, 4411-4422 (2019). https://doi.org/10.1007/s00170-019-03716-z

Xiang, Zhaowei; Wang, Ling; Yang, Chengli; Yin, Ming; Yin, Guofu, 2019. Analysis of the quality of slope surface in selective laser melting process by simulation and experiments. Optik 176, p. 68–77.

## Appendix A. Coefficient Tables of Model 1 and Model 2.

| Model 1: Term | Coefficient | Std Error |
|---|---|---|
| Constant | -7.5381 | 1.8541 |
| Scan speed v [mm/s] | -0.0014 | 0.0003 |
| Line energy E [J/mm] | -8.6043 | 3.1131 |
| Scan strategy | <1 df> | |
| ScStr_B_Chkonv | -0.5623 | 0.4563 |

| Model 2: Term | Coefficient | Std Error |
|---|---|---|
| Constant | -5.4718 | 2.7366 |
| Scan speed v [mm/s] | -0.0028 | 0.0012 |
| Line energy E [J/mm] | 31.8288 | 23.6124 |
| Spot diameter [µm] | 0.0666 | 0.0386 |
| Scan strategy | <1 df> | |

| | | |
|---|---|---|
| ScStr_B_CHkonvQ | 0.5623 | 0.4563 |
| Z rotation angle [°] | -0.0557 | 0.0266 |
| Bridge length l [mm] | 0.8332 | 0.0855 |
| Bridge heigth h_1 [mm] | 9.2723 | 2.1918 |
| Hatch distance [µm] | 0.1239 | 0.0252 |
| san speed [mm/s] * scan strategy | <1 df> | |
| ScStr_B_Chkonv | -0.0010 | 0.0002 |
| ScStr_B_CHkonvQ | 0.0010 | 0.0002 |
| Bridge length l [mm] * scan strategy | <1 df> | |
| ScStr_B_Chkonv | 0.3884 | 0.0764 |
| ScStr_B_CHkonvQ | -0.3884 | 0.0764 |
| Hatch distance [µm] * scan strategy | <1 df> | |
| ScStr_B_Chkonv | 0.0228 | 0.0045 |
| ScStr_B_CHkonvQ | -0.0228 | 0.0045 |
| Hatch distance [µm] * z rotation angle [°] | 0.0007 | 0.0003 |
| Bridge heigth h_1 [mm]^2 | -1.4941 | 0.5027 |
| Bridge heigth h_1 [mm] * hatch distance [µm] | -0.0589 | 0.0262 |

| | | |
|---|---|---|
| ScStr_B_Chkonv | 1.2472 | 0.7061 |
| ScStr_B_CHkonvQ | -1.2472 | 0.7061 |
| z rotation angle[°] | 0.0391 | 0.0189 |
| Bridge length l [mm] | 0.8829 | 0.0990 |
| Bridge height h_1 [mm] | 2.1751 | 2.2256 |
| Hatch distance [µm] | -0.0247 | 0.0448 |
| Scan speed [mm/s] * line energy [J/mm] | 0.01347 | 0.0075 |
| Line energy [J/mm]^2 | -168.4053 | 75.6400 |
| Scan strategy * line energy [J/mm] | <1 df> | |
| ScStr_B_Chkonv | -14.9226 | 2.8872 |
| ScStr_B_CHkonvQ | 14.9226 | 2.8872 |
| Spot diameter [µm]^2 | -0.0003 | 0.0001 |
| Scan strategy * spot diameter [µm] | <1 df> | |
| ScStr_B_Chkonv | -0.0163 | 0.0053 |
| ScStr_B_CHkonvQ | 0.0163 | 0.0053 |
| Bridge length l [mm] * scan strategy | <1 df> | |
| ScStr_B_Chkonv | 0.5074 | 0.0916 |
| ScStr_B_CHkonvQ | -0.5074 | 0.0916 |
| Bridge heigth h_1 [mm] * scan strategy | <1 df> | |
| ScStr_B_Chkonv | 0.8891 | 0.2929 |
| ScStr_B_CHkonvQ | -0.8891 | 0.2929 |
| Hatch distance [µm] * scan strateg | <1 df> | |
| ScStr_B_Chkonv | 0.0211 | 0.0055 |
| ScStr_B_CHkonvQ | -0.0211 | 0.0055 |
| Bridge heigth h_1 [mm] * z rotation angle [°] | -0.0394 | 0.0209 |
| Bridge heigth h_1 [mm]^2 | -2.3382 | 0.7625 |
| Bridge heigth h_1 [mm] * hatch distance [µm] | 0.0783 | 0.0416 |

## Appendix B. Coefficient Tables of Model 3 and Model 4

| Model 3: Term | Coefficient | Std Error |
|---|---|---|
| Constant | -6.2754 | 1.7183 |
| Scan speed v [mm/s] | -0.0009 | 0.0002 |
| Line energy E [J/mm] | -7.1703 | 3.1251 |
| Scan strategy | <1 df> | |
| ScStr_B_Chkonv | -0.5997 | 0.4675 |
| ScStr_B_CHkonvQ | 0.5997 | 0.4675 |
| Z rotation angle [°] | -0.0241 | 0.0097 |
| Bridge length l [mm] | 0.8181 | 0.0872 |
| Bridge height h_1 [mm] | 5.1730 | 1.4885 |
| Hatch distance [µm] | 0.1325 | 0.0222 |
| Scan speed [mm/s] * scan strategy | <1 df> | |
| ScStr_B_Chkonv | -0.0009 | 0.0002 |
| ScStr_B_CHkonvQ | 0.0009 | 0.0002 |
| Bridge length l [mm] * scan strategy | <1 df> | |
| ScStr_B_Chkonv | 0.3803 | 0.0782 |
| ScStr_B_CHkonvQ | -0.3803 | 0.0782 |
| Hatch distance [µm] * scan strategy | <1 df> | |
| ScStr_B_Chkonv | 0.0223 | 0.0045 |
| ScStr_B_CHkonvQ | -0.0223 | 0.0045 |
| Bridge heigth h_1 [mm] * z rotation angle [°] | 0.0274 | 0.0115 |
| Bridge heigth h_1 [mm] * hatch distance [µm] | -0.0590 | 0.0207 |

| Model 4: Term | Coefficient | Std Error |
|---|---|---|
| Constant | -0.6184 | 1.5804 |
| Line energy [J/mm] | -7.7602 | 2.9876 |
| Spot diameter [µm] | 0.0016 | 0.0061 |
| Scan strategy | <1 df> | |
| ScStr_B_Chkonv | 1.2099 | 0.7173 |
| ScStr_B_CHkonvQ | -1.2099 | 0.7173 |
| Z rotation angle [°] | 0.0356 | 0.0144 |
| Bridge length l [mm] | 0.1482 | 0.2752 |
| Bridge height h_1 [mm] | -0.4967 | 0.8104 |
| Hatch distance [µm] | 0.0667 | 0.0071 |
| Scan strategy * line energy [J/mm] | <1 df> | |
| ScStr_B_Chkonv | -14.9056 | 2.9297 |
| ScStr_B_CHkonvQ | 14.9056 | 2.9297 |
| Scan strategy * spot diameter [µm] | <1 df> | |
| ScStr_B_Chkonv | -0.0167 | 0.0054 |
| ScStr_B_CHkonvQ | 0.0167 | 0.0054 |
| Bridge length l [mm] * scan stategy | <1 df> | |
| ScStr_B_Chkonv | 0.4945 | 0.0928 |
| ScStr_B_CHkonvQ | -0.4945 | 0.0928 |
| Bridge heigth h_1 [mm] * scan strategy | <1 df> | |
| ScStr_B_Chkonv | 0.8899 | 0.2977 |
| ScStr_B_CHkonvQ | -0.8899 | 0.2977 |
| Hatch distance [µm] * scan strategy | <1 df> | |
| ScStr_B_Chkonv | 0.0223 | 0.0055 |
| ScStr_B_CHkonvQ | -0.0223 | 0.0055 |
| Hatch distance [µm] * z rotation angle [°] | -0.0003 | 0.0001 |
| Bridge heigth h_1 [mm] * bridge length l [mm] | 0.4780 | 0.1874 |